Figure S1

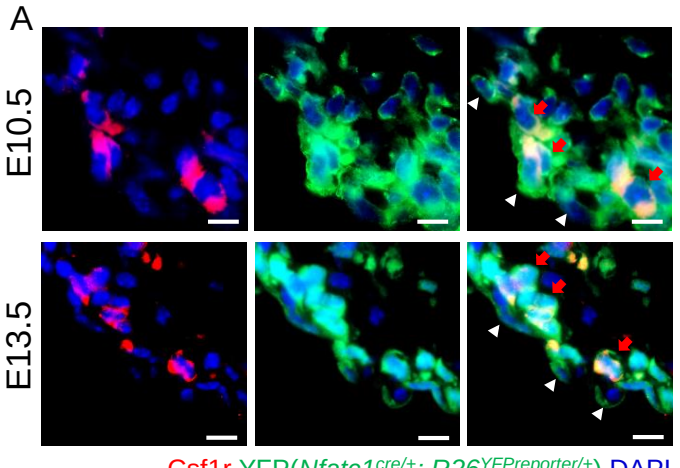

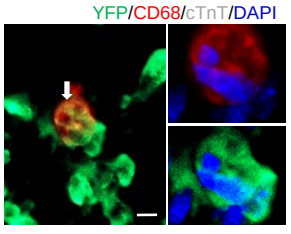

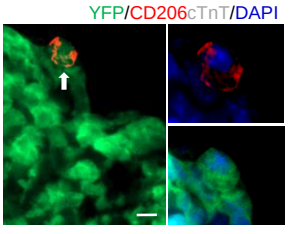

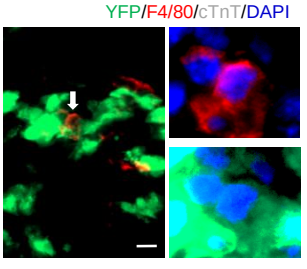

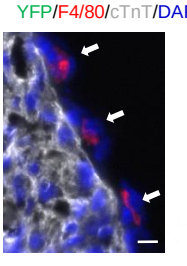

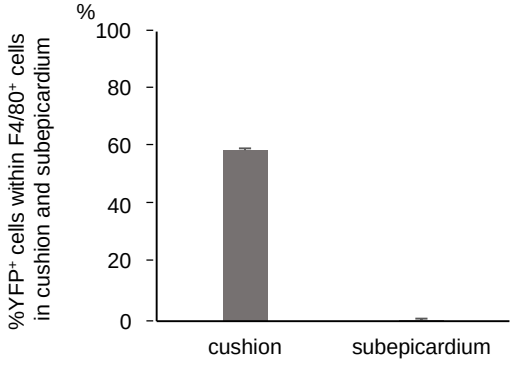

G

Counted cell number (X40)	Number in bar-graph
0	0
0-1	0.5
1	1
2	2
2-5	3
>5	4

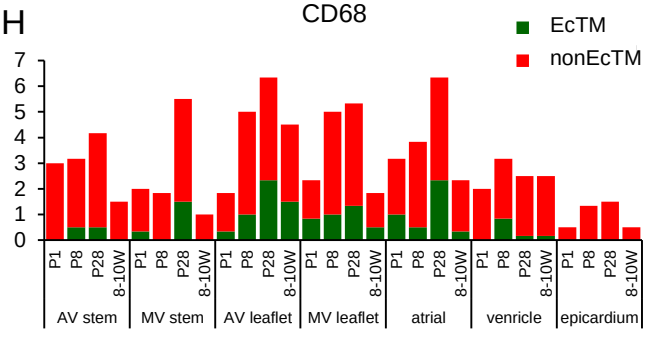

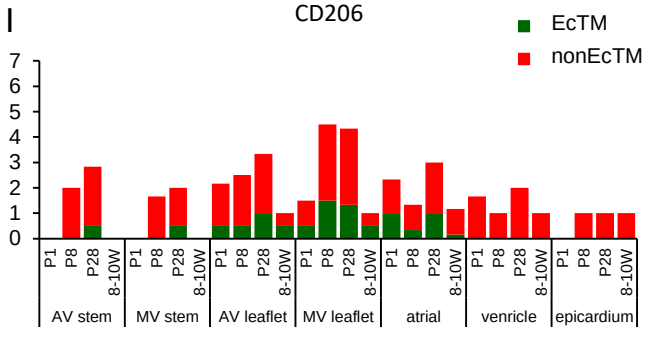

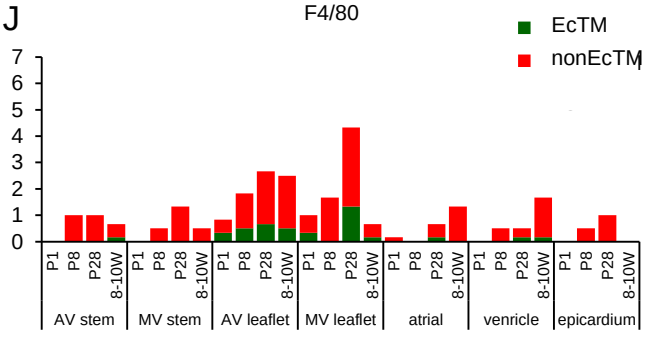

Figure S2

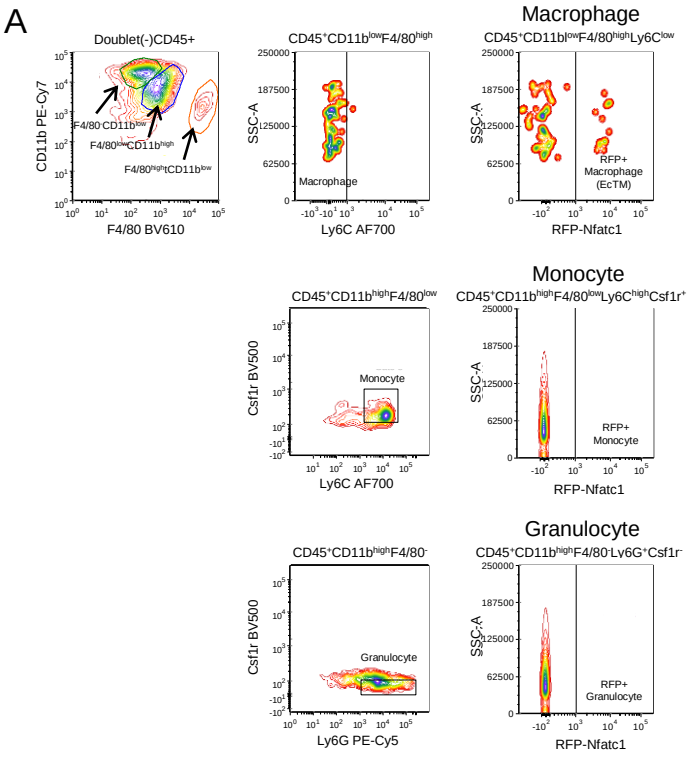
A
Doublet(-)CD45+
CD11b PE-Cy7
F4/80 BV610
F4/80-CD11blow
F4/80lowCD11bhigh
F4/80hightCD11blow
CD45+CD11blowF4/80high
SSC-A
Ly6C AF700
Macrophage
Macrophage
CD45+CD11blowF4/80highLy6Clow
RFP-Nfatc1
RFP+ Macrophage (EcTM)
Monocyte
CD45+CD11bhighF4/80lowLy6C+Csf1r+
Csf1r BV500
Monocyte
RFP+ Monocyte
Granulocyte
CD45+CD11bhighF4/80-Ly6G+Csf1r-
Ly6G PE-Cy5
Granulocyte
RFP+ Granulocyte

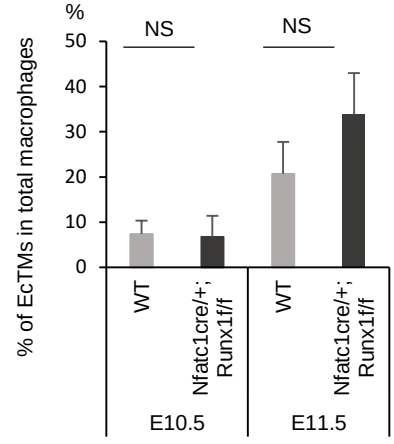
B
% of EcTMs in total macrophages
NS
NS
WT
Nfatc1cre/+; Runx1f/f
WT
Nfatc1cre/+; Runx1f/f
E10.5
E11.5

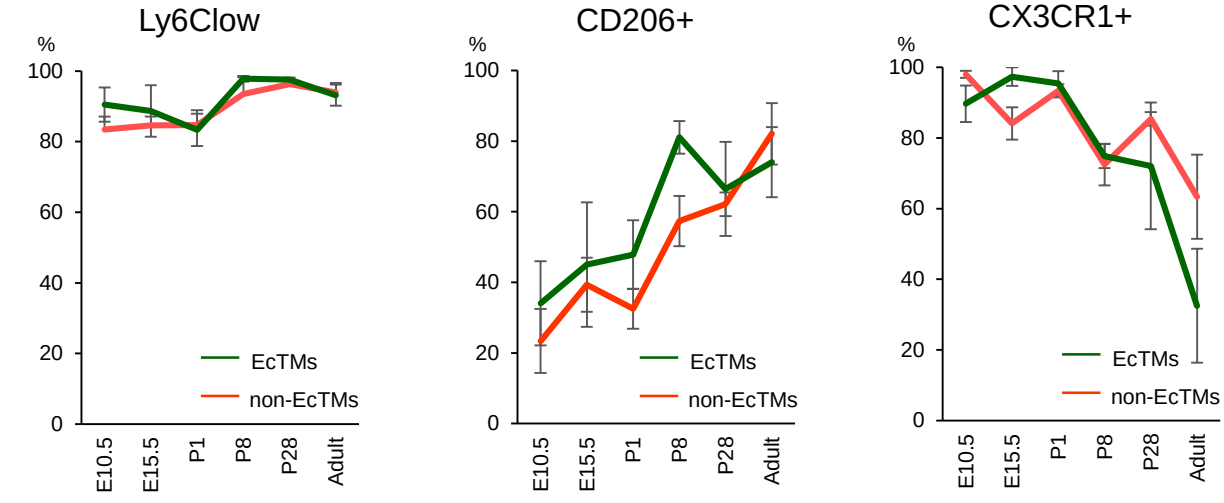
C
Ly6Clow
CD206+
CX3CR1+
%
EcTMs
non-EcTMs
E10.5
E15.5
P1
P8
P28
Adult

Figure S3

A

	Total Expected Pups	Total Experimental Pups
Csf1r$^{flox/+}$	35 (25%)	27 (19.3%)
Csf1r$^{flox/flox}$	35 (25%)	53 (37.9%)
Nfatc1$^{cre/+}$; *Csf1r*$^{flox/+}$	35 (25%)	40 (28.6%)
Nfatc1$^{cre/+}$; *Csf1r*$^{flox/flox}$	35 (25%)	20 **(14.2%)***
Total	140	140

*$P < 0.05$

B

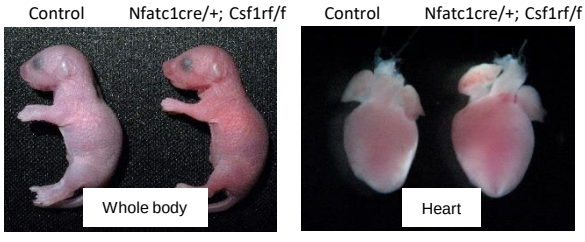

C

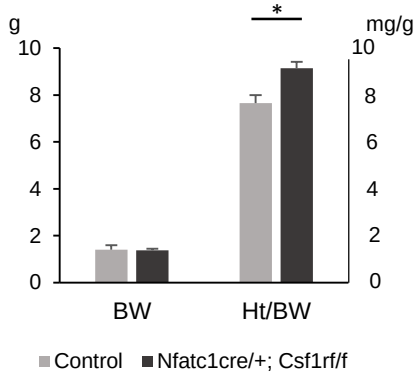

D

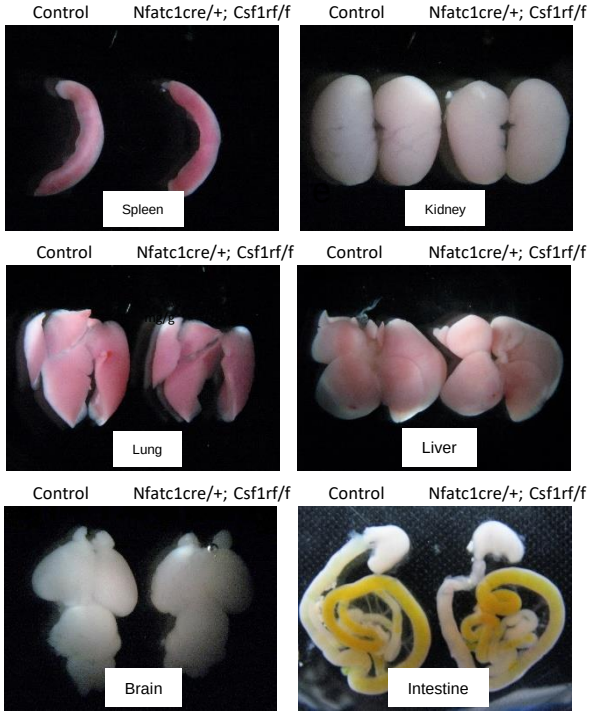

E

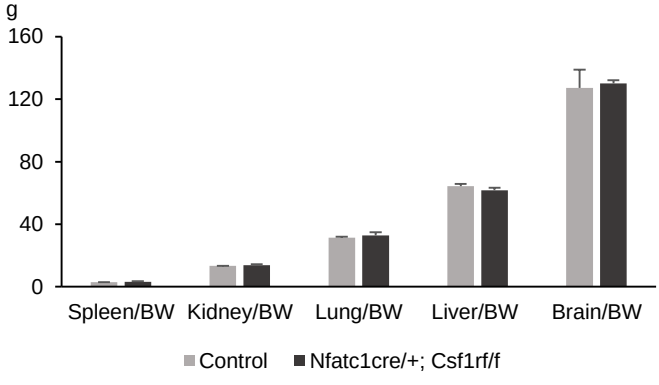

Figure S4

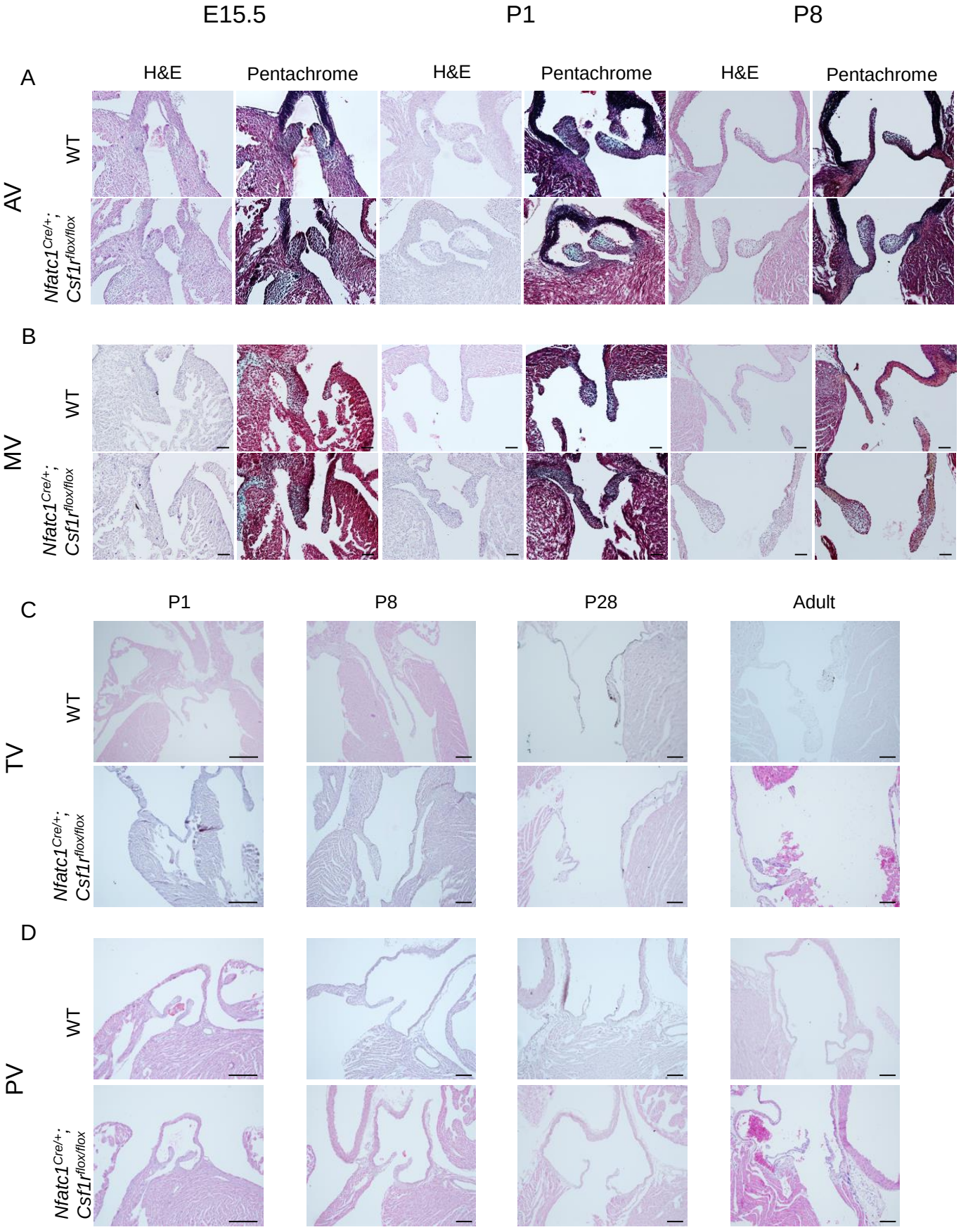
E15.5
P1
P8
A
H&E
Pentachrome
H&E
Pentachrome
H&E
Pentachrome
AV
WT
Nfatc1Cre/+; Csf1rflox/flox
B
MV
WT
Nfatc1Cre/+; Csf1rflox/flox
C
P1
P8
P28
Adult
TV
WT
Nfatc1Cre/+; Csf1rflox/flox
D
PV
WT
Nfatc1Cre/+; Csf1rflox/flox

Figure S5

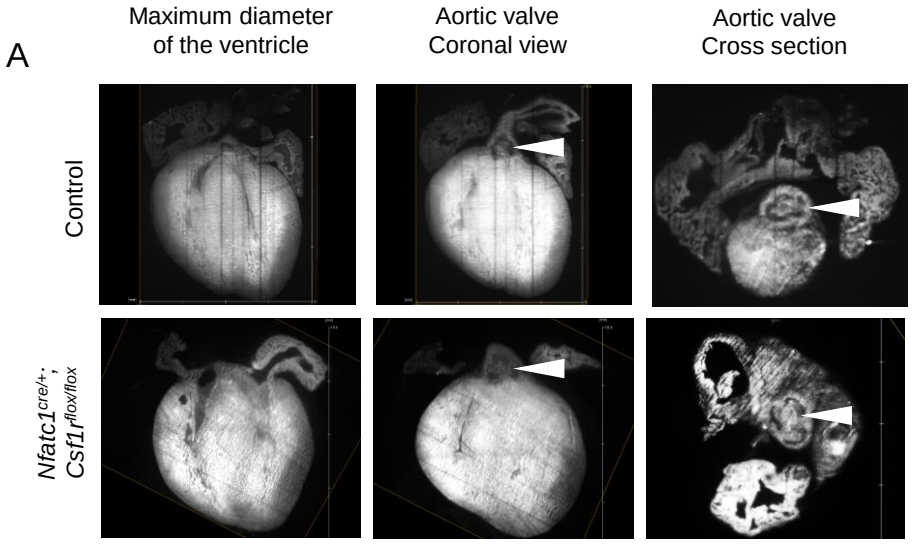
A
Maximum diameter of the ventricle
Aortic valve Coronal view
Aortic valve Cross section
Control
Nfatc1cre/+; Csf1rflox/flox

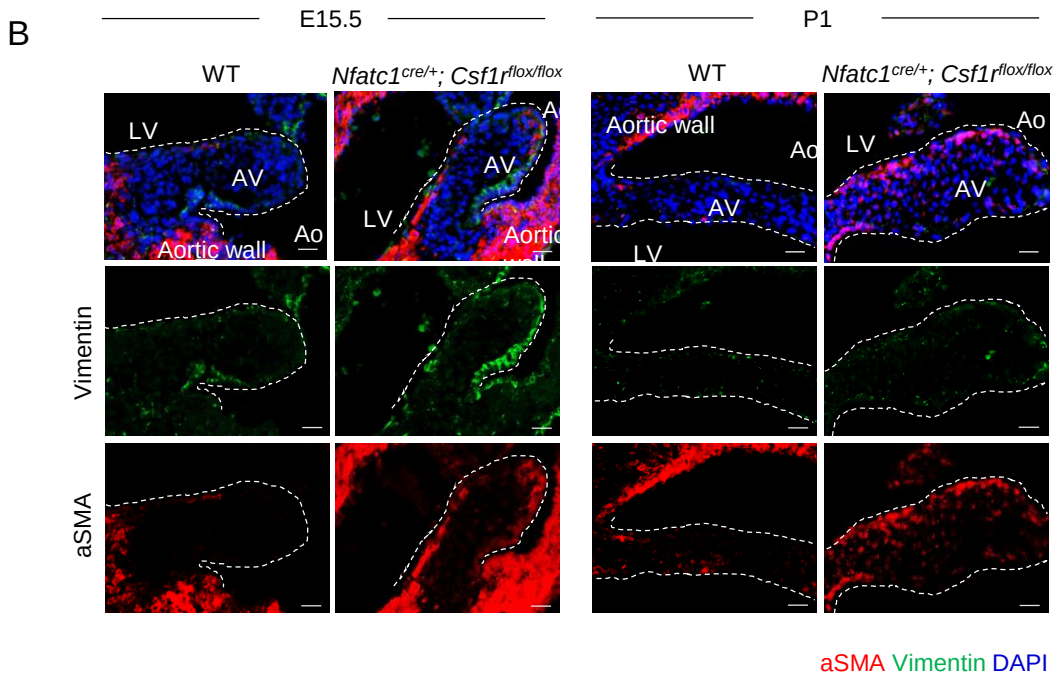
B
E15.5
P1
WT
Nfatc1cre/+; Csf1rflox/flox
WT
Nfatc1cre/+; Csf1rflox/flox
LV
AV
Aortic wall
Ao
Aortic wall
Ao
LV
AV
LV
Ao
AV
Vimentin
aSMA
aSMA Vimentin DAPI

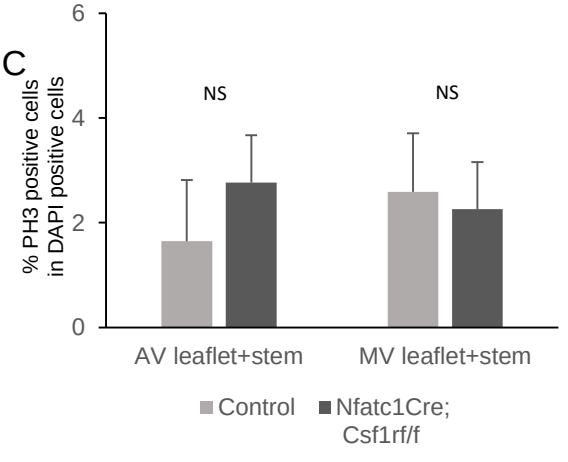
C
% PH3 positive cells in DAPI positive cells
6
4
2
0
NS
NS
AV leaflet+stem
MV leaflet+stem
Control
Nfatc1Cre; Csf1rf/f

Figure S6

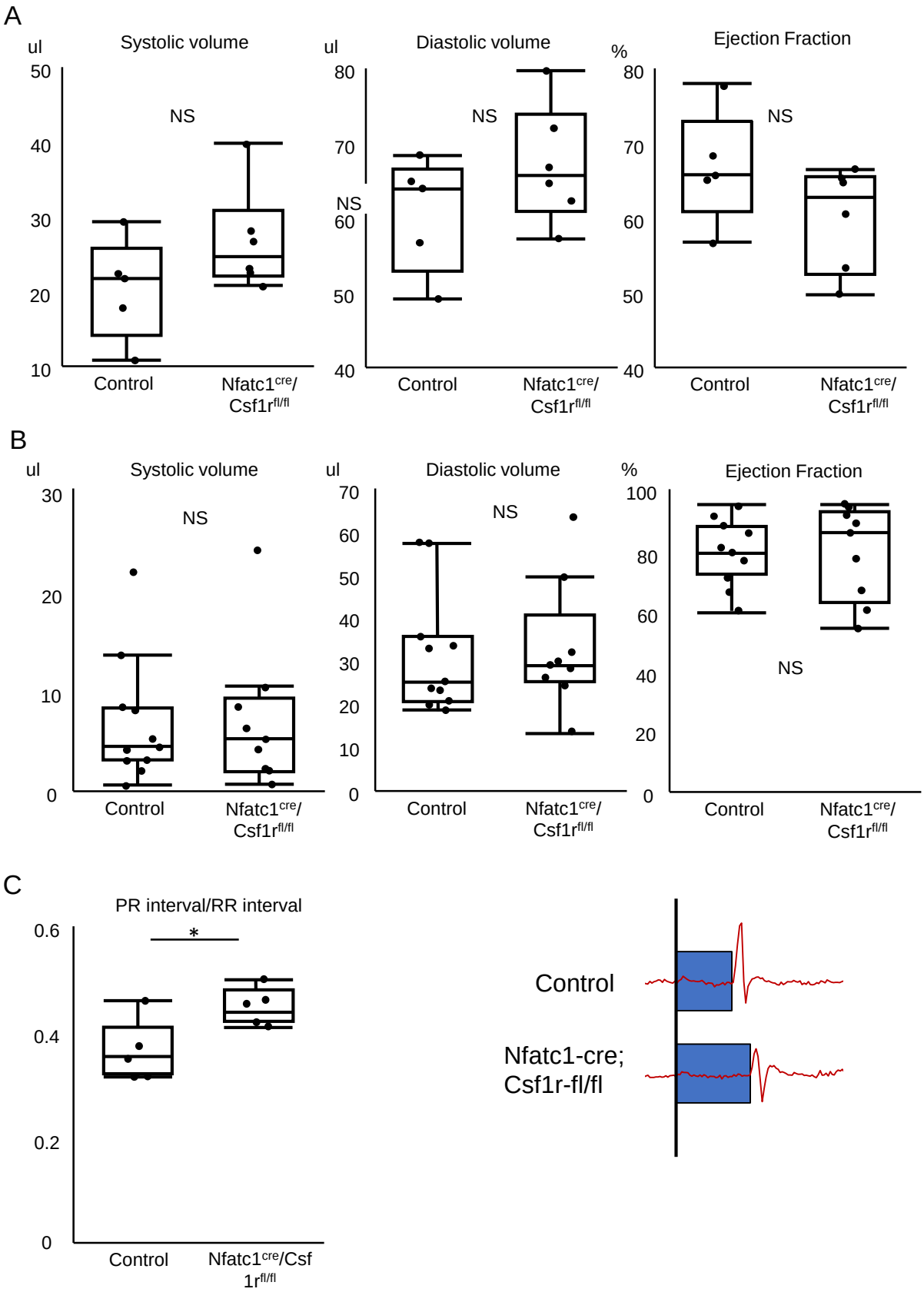
A
ul
Systolic volume
50
40
30
20
10
NS
Control
Nfatc1cre/
Csf1rfl/fl
ul
Diastolic volume
80
70
60
50
40
NS
NS
Control
Nfatc1cre/
Csf1rfl/fl
%
Ejection Fraction
80
70
60
50
40
NS
Control
Nfatc1cre/
Csf1rfl/fl
B
ul
Systolic volume
30
20
10
0
NS
Control
Nfatc1cre/
Csf1rfl/fl
ul
Diastolic volume
70
60
50
40
30
20
10
0
NS
Control
Nfatc1cre/
Csf1rfl/fl
%
Ejection Fraction
100
80
60
40
20
0
NS
Control
Nfatc1cre/
Csf1rfl/fl
C
PR interval/RR interval
0.6
0.4
0.2
0
*
Control
Nfatc1cre/Csf
1rfl/fl
Control
Nfatc1-cre;
Csf1r-fl/fl

Figure S7

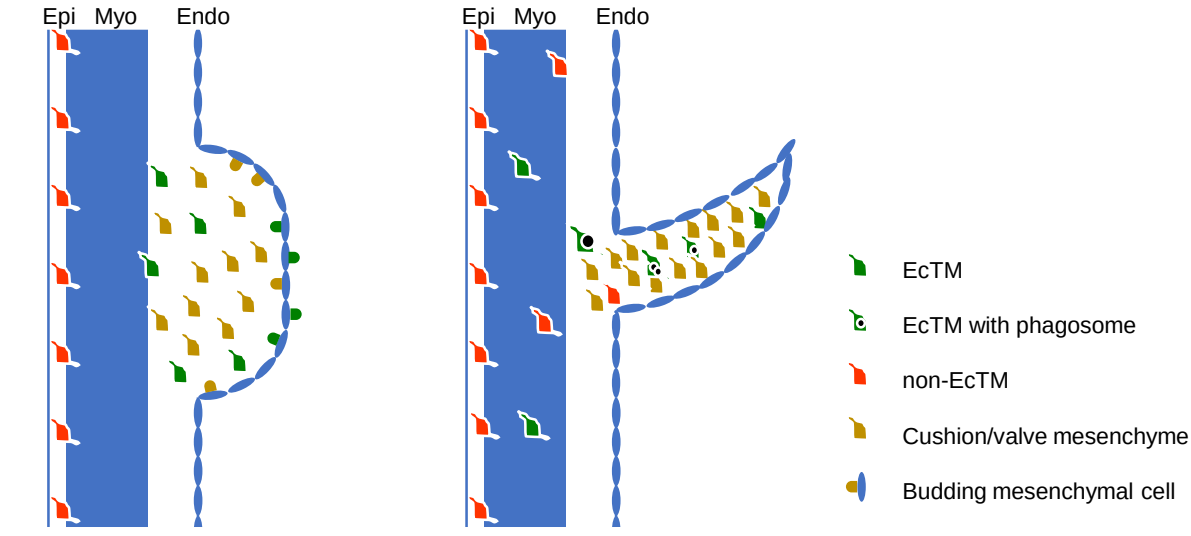

EMT
Generation of mesenchymal cells

Valve remodeling
Elimination of excessive cells.

Figure S1.

EcTMs exist in the endocardial cushion during embryonic stages and valvular structures at the postnatal stage. Related to Figure 3

A. Immunofluorescent staining for Csf1r of the cushion endocardium of *Nfatc1$^{cre/+}$; Rosa26$^{YFP\ reporter/+}$* mouse at E10.5 (top) and E13.5 (bottom). Csf1r^{+} YFP^{+} cells are found underneath the endocardial layer. Note that Csf1r signal was not detected in the endocardium (arrowhead). Scale bar = 10 μm.

B, C. Immunofluorescent staining for CD68 (d) and CD206 (e) (red) in addition to cTnT (white) and YFP (green) in the cushion mesenchyme of *Nfatc1$^{cre/+}$; Rosa26$^{YFP\ reporter/+}$* at E13.5.

D, E. Immunofluorescent staining for F4/80 (red), cTnT (white) and YFP (green) in the cushion (D) and subepicardium (E) of *Nfatc1$^{cre/+}$; Rosa26$^{YFP\ reporter/+}$* at E13.5.

F. The percentage of YFP cells in F4/80^{+} macrophages in the endocardial cushion and the subepicardium at E13.5 measured by ImageJ software. Note that EcTMs do not contribute significantly to the subepicardial macrophages.

G-J. Semi-quantitative analyses of endocardial contribution to the macrophages in different regions. (G) Method for semi-quantitative assessment. Contribution of endocardium to CD68 (H), CD206 (I) and F4/80 (J) macrophages in aortic valve (AV) stem, mitral valve (MV) stem, AV leaflet, MV leaflet, atria, ventricle, and epicardium. n=3, each.

Figure S2.

Contribution of Nfatc1-derived cells to hematopoietic subpopulations in embryonic tissues. Related to Figure 4 and 5

A. Representative flow cytometry plot for macrophages, monocytes, and granulocytes using *Nfatc1$^{cre/+}$; Rosa26 $^{Tomato/+}$* heart.

B. Flow cytometry quantification of %EcTMs in *Nfatc1$^{cre/+}$; Runx1$^{fl/fl}$* heart at E10.5 and 11.5. The number of EcTMs is not decreased in the mutants, suggesting that EcTMs are not dependent on Runx1. n = 4, 5, 3, 3 for WT E10.5, mutant E10.5, WT E11.5 and mutant E11.5, respectively.

C. Ly6C^{low}, CD206^{+}, and CX3CR1^{+} subsets of EcTMs and non-EcTMs during embryonic and postnatal development. n=3, each. Data represent mean ± SE. * $P < 0.05$ by Spearman's rank correlation.

Figure S3.

Gross morphology of *Nfatc1$^{cre/+}$; Csf1r$^{fl/fl}$* mutant organs. Related to Figure 7

A. The genotype of the pups from the breedings of *Nfatc1$^{cre/+}$; Csf1r$^{fl/+}$* and *Csf1r$^{fl/fl}$*. *Nfatc1$^{cre/+}$; Csf1r$^{fl/fl}$* pup are significantly underrepresented at weaning. $P < 0.05$ by χ^2 test.

B. Representative images of the embryos and hearts from control and *Nfatc1$^{cre/+}$; Csf1r$^{fl/fl}$* mice.

C. Body weight (BW) and heart weight (HW)/body weight (BW) comparison of control and *Nfatc1$^{cre/+}$; Csf1r$^{fl/fl}$* hearts. N = 2 and 4 for control and mutants, respectively. Data represent mean ± SE. * $P < 0.05$ by unpaired t-test.

D. Representative images of the spleen, kidney, lung, liver, brain, and intestine from control and *Nfatc1$^{cre/+}$; Csf1r$^{fl/fl}$* mice.

E. Organ weight per body weight (BW). No significant changes were found in the organ size other than the heart (**b**). N = 2 and 4 for control and mutants, respectively. Data represent mean ± SE.

Figure S4.
Valve histology of *Nfatc1$^{cre/+}$; Csf1r$^{fl/fl}$* embryos Related to Figure 7

A, B. H-E staining and Movat's pentachrome staining of aortic valve (AV; **A**) and mitral valve (MV; **B**) from the wild-type (WT) control and *Nfatc1$^{cre/+}$; Csf1r$^{fl/fl}$* adult mice. The thickening of AV and MV is obvious in mutants at P8, but the ECM pattern was preserved during fetal and neonatal stages. Scale bar = 50 μm

C, D. H-E staining of tricuspid (TV; **C**) and pulmonary (PV; **D**) valves of the control and *Nfatc1$^{cre/+}$; Csf1r$^{fl/fl}$* mice. Scale bar = 100 μm

Figure S5.
Valve phenotype of *Nfatc1$^{cre/+}$; Csf1r$^{fl/fl}$* mutants at perinatal stages Related to Figure 7

A. Light sheet imaging of the neonatal valves. Representative images of the 4-chamber section (left), coronal slice at the level of the aortic valve (middle), and cross section at the level of the aortic valve (right) of the hearts from *Nfatc1$^{cre/+}$; Csf1r$^{fl/fl}$* mouse and its wild-type littermate.

B. Activity of valvular interstitial cells in *Nfatc1$^{cre/+}$; Csf1r$^{fl/fl}$* hearts. Representative vimentin (green) and α-SMA (red) immunostaining of the aortic valves of the control and *Nfatc1$^{cre/+}$; Csf1r$^{fl/fl}$* mice at E15.5 (a) and P1 (b). Note that α-SMA staining is more intense in mutants at both E15.5 and P1.

C. pH3 staining of valve interstitial cells in *Nfatc1$^{cre/+}$; Csf1r$^{fl/fl}$* hearts.

Figure S6.
Cardiac function of *Nfatc1$^{cre/+}$; Csf1r$^{fl/fl}$* adult mice Related to Figure 7

A. Cardiac contractility measured by echocardiography.

B. Cardiac contractility measured by μMRI.

C. EKG analysis. PR interval was significantly prolonged in mutants.
Data represent mean ± SE. n = 5. *$P < 0.05$.

Figure S7.
Model for the role of endocardially-derived cardiac tissue macrophages
Related to Figure 1, 3, 5, 6 and 7
Mesenchymal cells are generated from cushion endocardium at E9.5-10.5. During this EMT process, tissue macrophages also arise from cushion endocardium (left). These endocardially-derived macrophages play a phagocytotic role to eliminate excessive mesenchymal cells, thereby facilitating valve remodeling.